ChemPubSoc Europe

DOI: 10.1002/cphc.201600354

CHEMPHYSCHEM Articles

DFT-Based Simulation and Experimental Validation of the Topotactic Transformation of MgAl Layered Double Hydroxides

Shi-Tong Zhang, Yibo Dou, Junyao Zhou, Min Pu, Hong Yan,* Min Wei,* David G. Evans, and Xue Duan[a]

The thermal topotactic transformation mechanism of MgAl layered double hydroxides (LDHs) is investigated by a combined theoretical and experimental study. Thermogravimetric differential thermal analysis (TG-DTA) results reveal that the LDH phase undergoes four key endothermic events at 230, 330, 450, and 800 °C. DFT calculations show that the LDH decomposes into CO_2 and residual O atoms via a monodentate intermediate at 330 °C. At 450 °C, the metal cations almost maintain their original distribution within the LDH(001) facet during the thermal dehydration process, but migrate substantially along the *c*-axis direction perpendicular to the (001) facet; this indicates that the metal arrangement/dispersion in the LDH matrix is maintained two-dimensionally. A complete collapse of the layered structure occurs at 800 °C, which results in a totally disordered cation distribution and many holes in the final product. The structures of the simulated intermediates are highly consistent with the observed in situ powder XRD data for the MgAl LDH sample calcined at the corresponding temperatures. Understanding the structural topotactic transformation process of LDHs would provide helpful information for the design and preparation of metal/metal oxides functional materials derived from LDH precursors.

1. Introduction

Layered double hydroxides (LDHs) are a class of minerals and synthetic materials represented by the general formula $[M^{II}_{1-x}M^{III}_{x}(OH)_2]^{x+}\cdot(A^{n-}_{x/n})\cdot m\,H_2O$, in which M^{II} and M^{III} are metal cations occupying octahedral positions in hydroxide layers, x is the molar ratio $M^{II}/(M^{II}+M^{III})$, and A denotes interlayer charge-compensating anions. The structure of LDHs is composed of stacks of alternating positively charged metal hydroxide (brucite-type) layers and negatively charged interlayer anions.[1–4] M^{II} includes Mg^{2+}, Zn^{2+}, Ni^{2+}, Fe^{2+}, Co^{2+}, and Ca^{2+}, and M^{III} includes Al^{3+}, Ga^{3+}, Fe^{3+}, and Cr^{3+}. The most common interlayer anions are CO_3^{2-}, halides, NO_3^-, SO_4^{2-}, and other inorganic anions, and x is normally between 0.2 and 0.4.[1,5–6] Recently, LDH materials have attracted considerable attention in the field of highly dispersed heterogeneous nanocatalysts due to their large versatility in chemical composition and structural architecture.[7–11] For example, nickel-based materials produced through the utilization of LDH precursors have been widely employed to catalyze the steam reforming of methanol or the hydrogenation of carbon oxides.[12,13] The topotactic transformation of LDHs occurring upon the calcination under reducing conditions plays a key role in the fabrication of supported metal nanocatalysts with specific surface structure and high dispersion.[13–16] Although much effort has been focused on the preparation of nanocatalysts through the LDH precursor approach, structural evolution (including metal migration, the dehydration process of host layers, and the formation mechanism of metal oxides) during the LDH thermal decomposition process is still not revealed clearly,[17–20] which limits the further development of LDH-based high-performance nanocatalysts. Therefore, a detailed understanding of the topotactic transformation of LDHs is essential and remains a challenging goal.

Several experimental studies on topotactic structural evolution in the thermal decomposition of LDHs have been performed;[16,21] these show that the decomposition process involves four main stages: the first step corresponds to the evaporation of weakly adsorbed surface and interlayer water, the second one is due to the removal of intercalated anions, the third one involves the dehydroxylation and collapse of the layered structure, and the final step is usually attributed to the formation of mixed-metal oxides (MMOs).[19,22,23] Petrov and Markov proposed "similar crystallographic correlations" between LDHs and the as-obtained metal oxides to define the topotactic decomposition of LDHs, and believed that metal distribution in the crystal lattice was a key issue in understanding the topotactic process.[16] Recently, some researchers deduced that the stacking of cations showed the largest density (compared with other facets) on the (00*l*) plane of LDH; therefore, during the topotactic decomposition of LDHs, oxide nucleation on the (00*l*) facet gave the lowest nucleation energy and led to the formation of the (111)-oriented metal oxides.[21]

[a] *Dr. S.-T. Zhang, Dr. Y. Dou, J. Zhou, Prof. M. Pu, Dr. H. Yan, Prof. M. Wei, Prof. D. G. Evans, Prof. X. Duan*
State Key Laboratory of Chemical Resource Engineering
Beijing University of Chemical Technology
Beijing 100029 (P.R. China)
E-mail: yanhong@mail.buct.edu.cn
weimin@mail.buct.edu.cn

Supporting Information and the ORCID identification number(s) for the author(s) of this article can be found under http://dx.doi.org/10.1002/cphc.201600354.

© 2016 Wiley-VCH Verlag GmbH & Co. KGaA, Weinheim

However, some key issues in the thermal structure evolution process are still unclear, for example, the formation of many secondary phases with poor crystallinity and the migration mechanism of metal cations.

Computational approaches offer an alternative option for investigating the topotactic transformation of LDHs during their thermal decomposition. For instance, density functional theory (DFT) has been used to elucidate the thermal reorganization of the interlayer carbonate over the temperature range 25–350 °C, and the results show that CO_3^{2-} anions graft to the host layer to form mono-/bidentate intermediates.[19] Moreover, DFT methods are frequently employed in studies of the chemically induced structural reconstruction of metal oxides/metal hydroxides.[24–27] However, computational studies on the LDH topotactic transformation are rarely performed and, in particular, have not been extended to explore the metal migration mechanism and the topotactic transformation process.[19] Therefore, a combined study based on experimental methods and theoretical calculations is a highly favorable approach to resolve this issue.

Herein, we focus on the topotactic transformation of MgAl–CO_3^{2-} LDH because it is the most typical LDH. We employed the DFT method to investigate the decomposition process of carbonate intercalated MgAl LDH, according to thermogravimetric differential thermal analysis (TG-DTA) in the temperature range 100–800 °C, including activation of the interlayer anions, identification of metal migration, and the decomposition mechanism. DFT-based molecular dynamics (MD) simulations are performed to provide atomic-scale insight into the structural evolution process of MgAl LDH. In situ powder XRD gives an experimentally observed structural change in the range 100–800 °C, which agrees well with the computational studies. The results show that, when the temperature is below 450 °C, metal arrangement/dispersion in the LDH matrix migrates substantially only along the *c*-axis direction, but the metal cations maintain their original arrangement well within the (001) facet. This work provides a fundamental understanding of structural evolution during the topotactic decomposition of LDHs, which gives helpful instructions in pursuit of effective fabrication of highly dispersed metal nanocatalysts.

2. Results and Discussion

2.1. Structure and Thermal Decomposition of LDHs Determined Experimentally

In situ XRD and TG-DTA are important methods in characterizing the thermal decomposition behavior of LDH materials, and supply information about crystal transitions and mass loss during temperature variation for the theoretical simulations. However, few reports combine in situ XRD and TG-DTA to investigate the thermal decomposition of carbonate-intercalated Mg_2Al LDH, although various experimental technologies have been used to monitor the structural evolution of LDH materials calcined at different temperatures.[19,28–32] The synthetic procedure strongly affects the crystallinity, purity, particle size, morphology, and cation ordering, and thus, has a large impact on the thermal behavior of the desired LDH materials.[33–35] Herein, the constructed calculation model is ideal with overall and local cation ordering, and we wish to obtain the synthesized LDH samples with high crystallinity and large particle size. Therefore, we chose the reported coprecipitation method through urea hydrolysis with hydrothermal treatment to prepare the LDH sample;[36] this has proved to be an effective method to obtain MgAl–CO_3 LDH compounds with high purity and crystallinity, owing to a gradual and uniform increase in the pH of the solution induced by urea hydrolysis.[37]

Figure 1 A shows the XRD pattern of the Mg_2Al–CO_3 LDH sample, which can be indexed as a hexagonal structure with 2q = 11.8, 23.7, 35.3, 39.7, 47.3, 61.1, and 62.3° (d_{003} = 7.49,

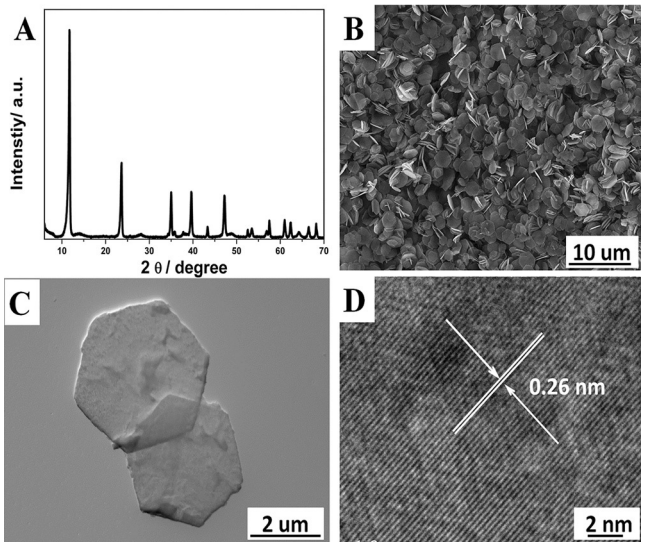

Figure 1. Characterization of the Mg_2Al–CO_3 LDH: A) powder XRD pattern, B) SEM image, C) TEM image, and D) the corresponding lattice fringes.

d_{006} = 3.75, d_{009} = 2.54, d_{012} = 2.27, d_{018} = 1.92, d_{110} = 1.52, and d_{112} = 1.49 Å, respectively). No other crystalline phase was detected, which indicated that the purity of the product was relatively high. However, this cannot exclude the existence of impurity phases because some impurity phases are amorphous, and therefore, they cannot be detected by XRD. The SEM image shows a narrow size distribution (2–2.3 mm) for the LDH. The TEM image reveals hexagonal LDH nanoplatelets (Figure 1 C) with lattice fringes corresponding to an interplanar distance of about 0.26 nm, which can be attributed to the (012) plane of the Mg_2Al–CO_3 LDH phase.

Simultaneous TG-DTA results for the Mg_2Al–CO_3 LDHs sample is shown in Figure 2. For the TG curves, at least 3 thermal events can be clearly distinguished up to 800 °C. The initial mass loss between 180 and 260 °C is 15.0 wt%, which is associated with the release of water molecules (physisorbed and crystallization water). Centered at 330 °C, the DTA curve (Figure 2) shows a unique endothermic event, corresponding to a mass loss of 10.0 wt% between 260 and 400 °C. This is related to the removal of intercalated water molecules and anionic species.[17,18] Further decomposition of the LDH sample

© 2016 Wiley-VCH Verlag GmbH & Co. KGaA, Weinheim

Figure 2. Simultaneous TG-DTA curves of the Mg_2Al–CO_3 LDH sample in the temperature range 100–800 °C.

at 450 °C can lead to the collapse of the 2D layered structure. The LDH sample undergoes a dehydration reaction with a weight loss of 19 wt% between 400 and 500 °C (Figure 2). Subsequently, a contiguous weight loss between 500 and 800 °C (5.0 wt%) is due to the dehydroxylation of host layers. Valente et al. have studied the TG-DTA properties of carbonate-intercalated Mg_2Al LDHs in detail.[18] Although the results of this work are not in good agreement with their report (mainly due to the distinguishably different morphology, particle size, and crystallinity), the TG data also reveals four general events at 25–250, 250–350, 350–550, and 550–700 °C. The TG-DTA results suggest four key points at 230, 330, 450, and 800 °C, and recent advances have clearly demonstrated that the thermal decomposition of Mg_2Al–CO_3 LDH at about 200 °C is related to the removal of interlayer water molecules.[19] Furthermore, the enthalpy change associated with the release of water from carbonate-intercalated Mg_2Al LDH was calculated, and the resulting value (0.47 eV per molecule) agreed well with the experimental result (0.45–0.57 eV per molecule).[34] This indicates that the employed method for calculating the free energy is reliable. In addition, the TG experiments for MgAl LDH at a heating rate of 5 °C min^{-1} (Figure S1 in the Supporting Information) were performed. Compared with the TG curves in Figure 2 at a heating rate of 2 °C min^{-1}, the influence of the heating rate on the TG experiments for Mg_2Al–CO_3 LDH was not significant. MD simulation studies were performed at 330, 450, and 800 °C to investigate the thermal decomposition behavior of Mg_2Al–CO_3 LDH.

2.2. Calculated Three Steps of LDH Decomposition

MD simulations showed that the studied systems reached equilibrium with structures and free energies fluctuating around constant values within 0–10 ps (Figure S2 in the Supporting Information). The temperatures adopted were 330, 450, and 800 °C (Figure 3), respectively; these values were determined by the TG-DTA results in this study.

Although the weight-loss event of the LDH at around 200–500 °C has been ascribed to the release of interlayer carbonate and hydroxyl groups of host layers, the mechanism of this process is very controversial and not well established. Rives proposed that this process was the direct decomposition of the interlayer carbonates, producing CO_2 and residual oxygen species into the layers.[29] Recent reports experimentally suggested two possible grafting intermediates of carbonate anion: the mono- (Figure S3 B in the Supporting Information) and bidentate states (Figure S3C in the Supporting Information).[19,35,36] Herein, dynamic simulations and frequency analysis were performed on the basis of models constructed to provide theoretical insights into the decomposition process of interlayer CO_3^{2-}. The calculated reactions are given by Reactions (1)–(5):

$$Mg_8Al_4(OH)_{24}\cdot 2\,CO_{3(s)} \rightarrow Mg_8Al_4(OH)_{24}\cdot O\cdot CO_{3(s)} + CO_{2(g)} \quad (R1)$$

$$Mg_8Al_4(OH)_{24}\cdot 2\,CO_{3(s)} \rightarrow Mg_8Al_4(OH)_{22}\cdot O\cdot 2\,CO_{3(s)} + H_2O_{(g)} \quad (R2)$$

$$Mg_8Al_4(OH)_{22}\cdot O\cdot 2\,CO_{3(s)} \rightarrow Mg_8Al_4(OH)_{22}\cdot 2\,O\cdot CO_{3(s)} + CO_{2(g)} \quad (R3)$$

$$Mg_8Al_4(OH)_{22}\cdot O\cdot 2\,CO_{3(s)} \rightarrow Mg_8Al_4(OH)_{20}\cdot 2\,O\cdot 2\,CO_{3(s)} + H_2O_{(g)} \quad (R4)$$

$$Mg_8Al_4(OH)_{20}\cdot 2\,O\cdot 2CO_{3(s)} \rightarrow Mg_8Al_4(OH)_{20}\cdot 4\,O_{(s)} + 2\,CO_{2(g)} \quad (R5)$$

The fabrication of heterogeneous catalysts with high dispersion and excellent stability by calcining LDH precursors is usually achieved in the temperature range from 400 to 500 °C.[13,37] Moreover, the MgAl-LDHs calcined in this temperature range can recover their original layered structure with the presence of water and anions (memory effect).[42,43] When calcined in the temperature range 800–1000 °C, the LDHs decompose to give MMOs and spinels without the memory effect.[39] To further understand structural changes to LDHs during the decomposition process at 450 °C, the intermediate phase produced by interlayer CO_3^{2-} decomposition is calculated by MD simulations of 30 ps at 450 °C. Reactions (6)–(12) are taken into consideration:

$$Mg_8Al_4(OH)_{20}\cdot 4\,O_{(s)} \rightarrow Mg_8Al_4(OH)_{18}\cdot 5\,O\ (CLDH\text{-}1,s) + H_2O_{(g)} \quad (R6)$$

$$CLDH\text{-}1_{(s)} \rightarrow Mg_8Al_4(OH)_{16}\cdot 6\,O\ (CLDH\text{-}2,s) + H_2O_{(g)} \quad (R7)$$

$$CLDH\text{-}2_{(s)} \rightarrow Mg_8Al_4(OH)_{14}\cdot 7\,O\ (CLDH\text{-}3,s) + H_2O_{(g)} \quad (R8)$$

$$CLDH\text{-}3_{(s)} \rightarrow Mg_8Al_4(OH)_{12}\cdot 8\,O\ (CLDH\text{-}4,s) + H_2O_{(g)} \quad (R9)$$

$$CLDH\text{-}4_{(s)} \rightarrow Mg_8Al_4(OH)_{10}\cdot 9\,O\ (CLDH\text{-}5,s) + H_2O_{(g)} \quad (R10)$$

$$CLDH\text{-}5_{(s)} \rightarrow Mg_8Al_4(OH)_{8}\cdot 10\,O\ (CLDH\text{-}6,s) + H_2O_{(g)} \quad (R11)$$

$$CLDH\text{-}6_{(s)} \rightarrow Mg_8Al_4(OH)_{6}\cdot 11\,O\ (CLDH\text{-}7,s) + H_2O_{(g)} \quad (R12)$$

The memory effect of the LDHs was also simulated by intercalating water and CO_2 molecules one by one into the six

© 2016 Wiley-VCH Verlag GmbH & Co. KGaA, Weinheim

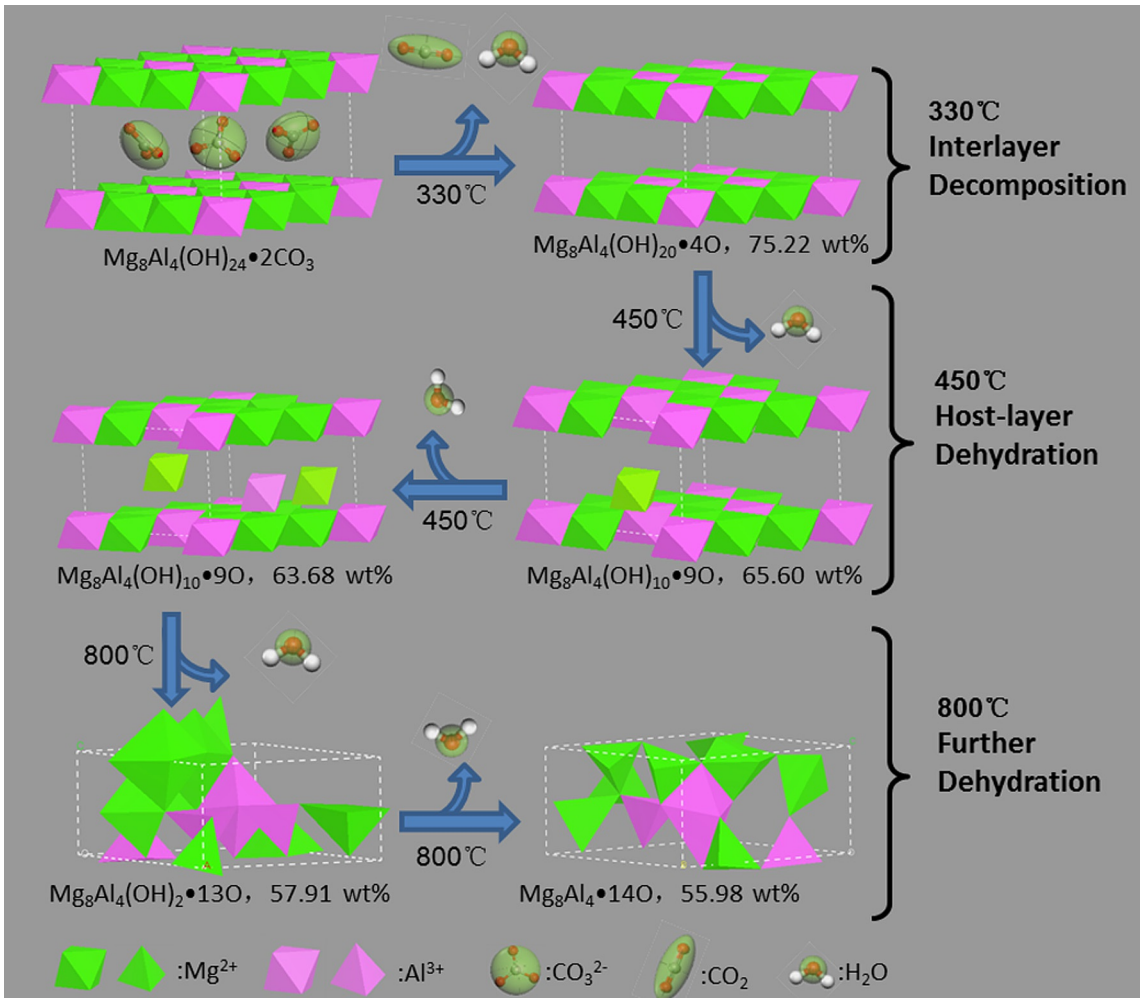

Figure 3. Schematic representation of the calculated three steps for the thermal decomposition of LDHs.

models of calcined LDH (CLDH-1–CLDH-6), respectively, and the MD simulations were performed to relax these structures.

The structure of CLDH-7 was further dynamically simulated at 800 °C, followed by dehydration to CLDH-8 ($H_4O_{16}Mg_8Al_4$), -9 ($H_2O_{15}Mg_8Al_4$), and -10 ($H_2O_{15}Mg_8Al_4$), as described by dehydration Reactions (13)–(15):

$$CLDH\text{-}7_{(s)} \rightarrow Mg_8Al_4(OH)_4 \cdot 12\,O\ (CLDH\text{-}8,s) + H_2O_{(g)} \quad (R13)$$

$$CLDH\text{-}8_{(s)} \rightarrow Mg_8Al_4(OH)_2 \cdot 13\,O\ (CLDH\text{-}9,s) + H_2O_{(g)} \quad (R14)$$

$$CLDH\text{-}9_{(s)} \rightarrow Mg_8Al_4 \cdot 14\,O\ (CLDH\text{-}10,s) + H_2O_{(g)} \quad (R15)$$

In this study, although the canonical ensemble (*NVT*) was used in the simulation, because this is a solid-phase reaction at certain temperatures, the pressure can be viewed as a constant. In the case of the gas phase involved, the volume of gas molecules is determined according to the equation $V=nRT/p$, in which p is always set to be 0.1 MPa. Therefore, the variation of the Gibbs free energy (DG) is employed to judge the spontaneity of a reaction [Eq. (1)]:

$$DG = \sum n_P G_P - \sum n_R G_R \quad (1)$$

in which n_p and n_R are the stoichiometric coefficients for products and reactants, respectively; and G_p and G_R are the calculated Gibbs free energies of products and reactants, respectively. The Gibbs free energy of each intermediate is calculated according to $G=H-TS$ based on the structure obtained from MD simulations (for details, see the Supporting Information: Calculation of Gibbs free energy).[44–49]

2.3. DFT Simulation of the Decomposition of Interlayer CO_3^{2-} at 330 °C

As discussed in Section 2.2, three mechanisms for the release of the interlayer carbonates have been proposed: direct decomposition and decomposition via mono- or bidentate intermediates. To identify the intermediate of the initial decomposition of LDHs at 330 °C, MD simulations were performed after optimization of three representative models, namely, carbonate (C-LDH), monodentate (Mono-LDH), and bidentate (Bi-LDH). The bulk model of Mg_2Al–CO_3 LDH without any water molecules in the unit cell was optimized, and the removal of interlayer water leads to a decrease of the basal spacing from 7.48 to 6.77 Å, in agreement with the in situ XRD results. In the case of Mono-LDH, nine possible initial incorporated structures

© 2016 Wiley-VCH Verlag GmbH & Co. KGaA, Weinheim

were taken into consideration, and the optimized structure in which two interlayer carbonates coupled with different host layers (Figure S4 in the Supporting Information) showed the lowest calculated free energy. In the Bi-LDH system, carbonate can only bind with octahedral Mg^{2+}, since the incorporated structure of Al^{3+} finally evolves to form the monodentate model after 5 ps of simulation, according to our simulation. In the dynamic simulation trajectory of C-LDH, direct transformation from C-LDH to Mono-LDH is not observed, but the transformation from C-LDH to Mono-LDH produces a slightly negative D*G* (−0.04 eV). This indicates that the interlayer carbonates can spontaneously incorporate into the host sheets to form the intermediate structure of Mono-LDH at 330 °C. The structure of Bi-LDH, which has been experimentally detected in the studies on the LDHs dis-/adsorbing CO_2,[35,50] however, is not favorable under these conditions. This is because the Gibbs free energy of Bi-LDH is higher than that of C-LDH by about 0.43 eV. Because D*G* is a function of temperature and may become negative with increasing temperature, the MD simulations of C-LDH and Bi-LDH were extended to 300, 370, 410, and 450 °C, to confirm whether the formation of the bidentate configuration was favorable or not during the initial activation of the MgAl LDH. According to the calculation results, the transformation from C-LDH to Bi-LDH is still not thermodynamically allowed (Table S1 in the Supporting Information). Costa et al. systematically studied the initial steps of thermal decomposition for Mg_2Al LDH by means of an ab initio method, and they also found that the formation of Bi-LDH from C-LDH produced a positive D*G* in the temperature range 25–350 °C.[19] The results imply that the initial decomposition of intercalated CO_3^{2-} occurs via the Mono-LDH intermediate rather than the Bi-LDH at 330 °C.

The decomposition of the intermediate Mono-LDH was further simulated at 330 °C, and the calculated results are summarized in Figure 5. For Mono-LDH, two hydroxyl groups are exchanged into the interlayer region by the incorporated CO_3^{2-} (Figure 4B and E). In the MD simulation, these interlayer hydroxyl groups reversibly react with hydrogen atoms in the host sheets and produce interlayer water molecules. The release of one of these H_2O molecules produces a negative D*G* of −0.10 eV at 330 °C (reaction R2 in Figure 5), whereas the escape of one CO_2 molecule from Mono-LDH results in a D*G* value of 0.05 eV (reaction R1 in Figure 5). This indicates that the decomposition of the Mono-LDH intermediate starts with the removal of produced water. The D*G* value for the second water release is −0.06 eV, but the removal of an interlayer CO_2 still presents a positive D*G* value (0.16 eV), as shown in Figure 5C–E. After the dehydration process, the interlayer CO_2 can spontaneously escape into the air, according to the D*G* values (−0.11 and −0.25 eV). Because, for the first two steps of the

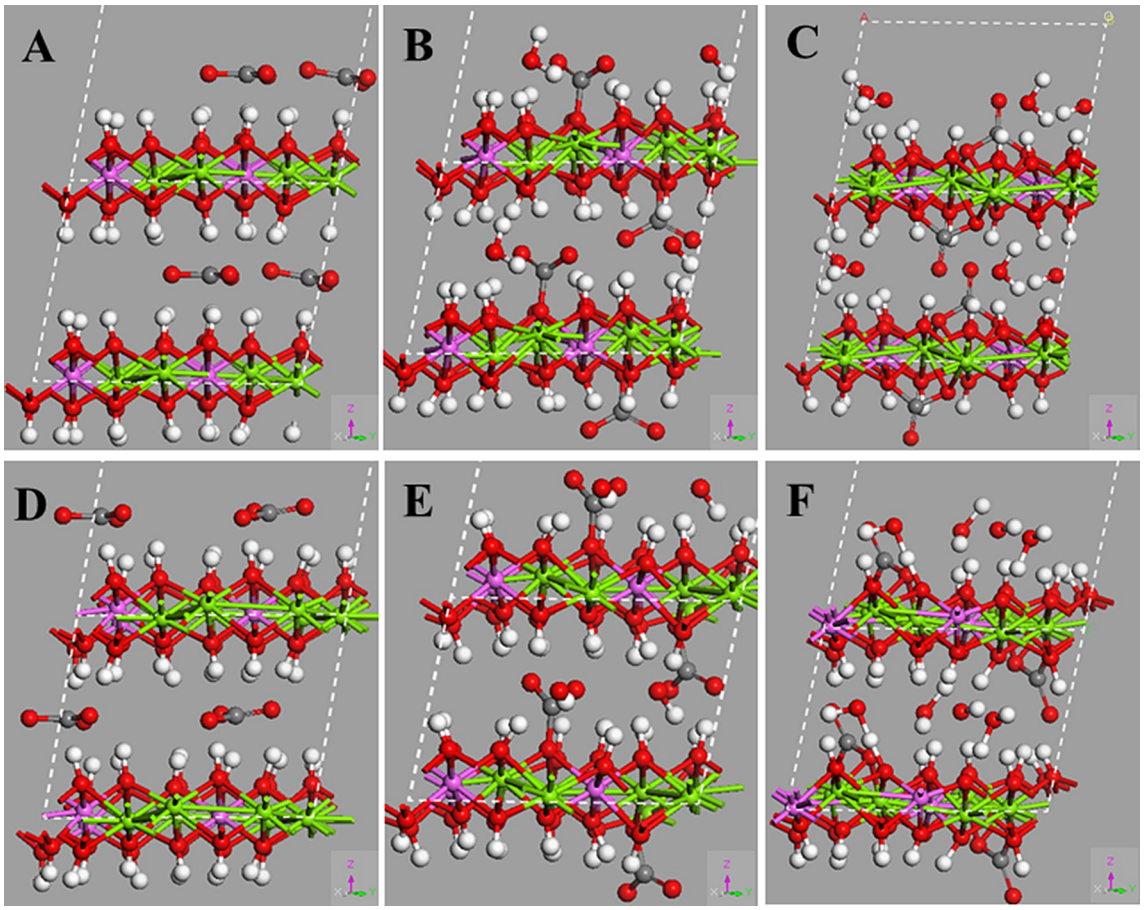

Figure 4. DFT-optimized models of A) C-LDH, B) Mono-LDH, and C) Bi-LDH, and snapshots of the *NVT* (330 °C) at 30 ps for dynamic simulations of D) C-LDH, E) Mono-LDH, and F) Bi-LDH (white, H; gray, C; red, O; green, Mg; pink, Al).

© 2016 Wiley-VCH Verlag GmbH & Co. KGaA, Weinheim

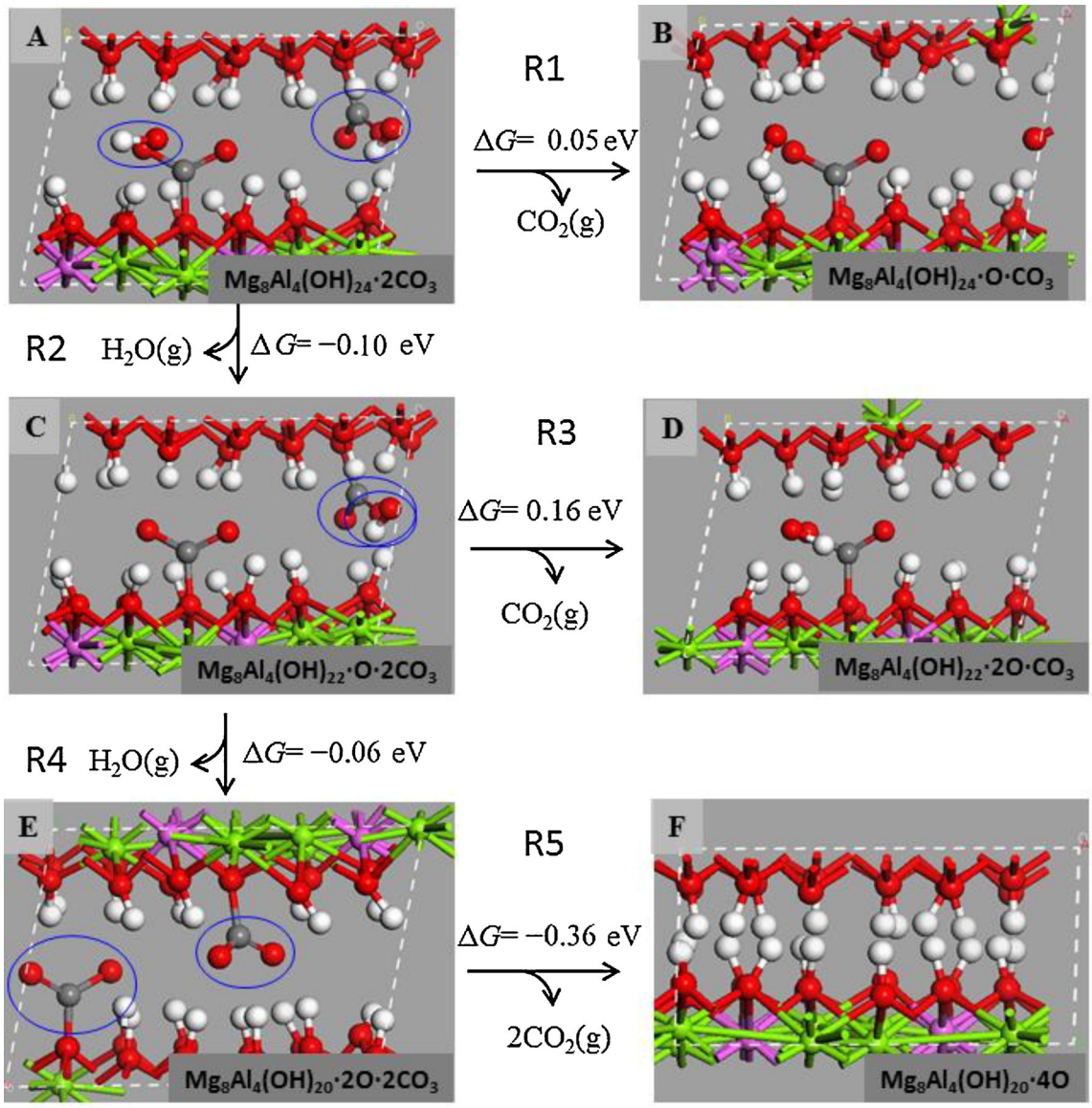

Figure 5. Decomposition process of Mono-LDH, denoted with D*G* and D*H* at 330 °C (white, H; gray, C; red, O; green, Mg; pink, Al).

decomposition of the intermediate Mono-LDH, the D*G* values for water release are negative and that of the removal of an interlayer CO_2 are positive (Figure 5), it can be deduced that water release occurs prior to the removal of CO_2. However, it is noteworthy that the concomitant release of water and CO_2 in the experimental calcination of LDHs is still practicable,[51,52] because of the existence of defects and inhomogeneity in heating. The gallery distance of the LDH material decreases to 4.42 Å after the decomposition of the interlayer anions, with the corresponding loss weight of 24.8 wt%. The results are in good agreement with the TG-DTA data (25 wt%).

2.4. DFT Simulation of the Dehydration of Host Layers at 450 °C

The product of interlayer CO_3^{2-} decomposition at 330 °C is further gradually heated up to 450 °C by a MD simulation on the timescale of 30 ps and then equilibrated at 450 °C for another 30 ps. During equilibration of the MD simulations, two hydrogen atoms in the host sheets reversibly bond to a neighboring oxygen atom to produce a water molecule. After removing this water molecule, the component of the structure becomes $Mg_8Al_4(OH)_{18}O_5$ (CLDH-1, Figure 6 A). This procedure is supported by the fact that any water molecules formed can rapidly desorb from the interlayer region at temperatures above 230 °C.[17] MD simulation results based on CLDH-1 at 450 °C show that the material still maintains a brucite-like structure, and five O^{2-} are dispersed in the LDH (001) facet. The distance between neighboring Mg^{2+} in CLDH-1 ranges from 2.78 to 3.15 Å, with an average value of 3.04 Å, which is slightly larger than that in an ideal LDH structure [(3.01 ± 0.01) Å]. The H–O–H configuration still appears during equilibration of the MD simulation for CLDH-1 and is removed to produce the model of CLDH-2 ($Mg_8Al_4(OH)_{16}O_6$). The MD simulation is performed on the basis of CLDH-2, and the equilibrated result shows that the layered structure is well maintained (Figure 6 B). After the

© 2016 Wiley-VCH Verlag GmbH & Co. KGaA, Weinheim

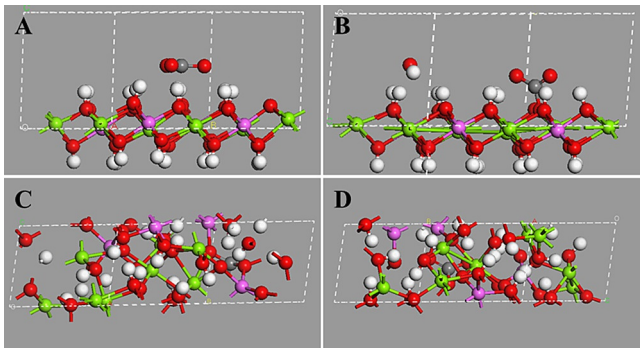

Figure 7. Snapshots at 30 ps of the *NVT* (25 °C) dynamic simulations of the CLDH-1 and CLDH-5 structure reconstruction when intercalating A) H_2CO_3 and B) CO_2+H_2O, as well as the memory effect of CLDH-6 by intercalating C) H_2CO_3 and D) CO_2+H_2O (white, H; gray, C; red, O; green, Mg; pink, Al).

molecule breaks, and the equilibrium configuration displays a very typical LDH structure (Figure 7A). When adding the interlayer water and one CO_2 molecule into $Mg_8Al_4(OH)_{20}O_4$, a Mono-LDH (Figure 7B) is also obtained, which can be converted into LDHs. However, for nonlayered CLDH-6, no reconstruction process from calcined LDH to the original LDH is observed (Figures 7C and 7D); moreover, direct intercalation of a CO_2 molecule into CLDH-6 does not result in a layered structure. This suggests the disappearance of the memory effect accompanied by a structural change when LDHs are calcined up to CLDH-6. Interestingly, the experimentally observed intermediate formed during the calcination process of LDH, with a bidentate configuration, is theoretically found in the study of the memory effect by dynamic simulation of CLDH-4 and –5 models with CO_2 first inserted at 450 °C. Ritter et al. investigated the formation of mono- and bidentate structures during CO_2 adsorption and release from LDHs at 450 °C, and found that the density of the active sites (O^{2-}) substantially affected the formation of mono- and bidentate intermediates.[50] Clearly, the high density of O^{2-} in CLDH-4/-5 models induces the formation of the bidentate configuration when CO_2 is adsorbed into the interlayer gallery.

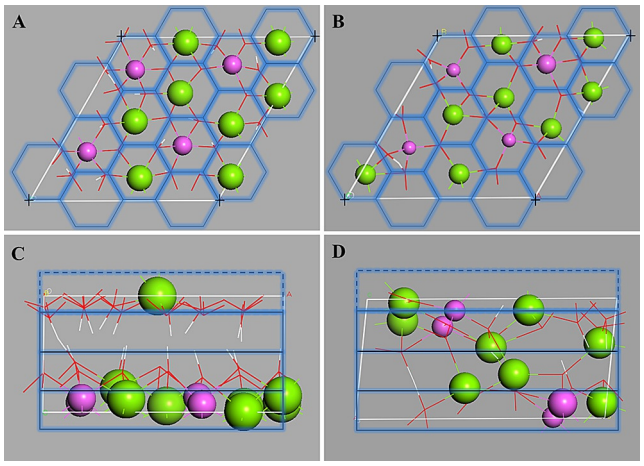

Figure 8. Top views of A) CLDH-1 and B) CLDH-6; side views of C) CLDH-1 and D) CLDH-6. The cell used to calculate the values of s is defined by the blue line, and the blue dashed line represents the imaginary neighbor cell (white, H; gray, C; red, O; green, Mg; pink, Al).

To further understand structural evolution of the LDH during its thermal decomposition process, the distribution degree (s) and root-mean-square deviation (rmsd) of metal cations are defined by the LDH (001) and (120) facets, respectively. As shown in Figure 8A, the (001) facet of CLDH-1 was divided into 12 hexagonal cells with each metal atom located at the cell center. The distribution degree of metal atoms in the LDH (001) facet (top view) is defined by Equation (2):

$$s_{top} = \sqrt{\frac{\sum_{i=1}^{12}\left(X_{top,i} - \bar{X}_{top}\right)^2}{12}} \quad (2)$$

in which X_{top} is the amount of metal atom in the *i*th cell ($i=1$–12); $\bar{X}_{top}$ is the average number of metal atoms in each cell ($\bar{X}_{top}=1$ in the case of the LDH (001) facet). The lattice of the LDH (120) facet (side view) was divided into three parts along the *c* axis because the height of the model was approximately three times the average diameter of Mg^{2+} and Al^{3+} (Figure 8C). The distribution degree of Mg and Al in the side view of the CLDH model is defined by Equation (3):

$$s_{side} = \sqrt{\frac{\sum_{i=1}^{3}\left(X_{side,i} - \bar{X}_{side}\right)^2}{3}} \quad (3)$$

in which $\bar{X}_{side}=4$ for the LDH (120) facet; the radius of the metal cations were determined by Shannon[53] when computing the amount of metals in each cell. These definitions use standard deviations in statistical theory for reference; these measure the amount of dispersion from the average distribution in each cell. A low value of s indicates that the metal atoms tend to be averagely spread across the corresponding facet, and a high s implies that the metal atoms are concentrated in minority cells. The rmsd is defined by Equation (4):

$$rmsd = \sqrt{\frac{\sum_{i=1}^{12} s_i^2}{12}} \quad (4)$$

in which s_i denotes the displacement of the *i*th metal atom (the initial LDH model is used as a reference). The values of

Table 1. Summary of the values of s_{top}, s_{side}, $rmsd_{top}$, and $rmsd_{side}$ for CLDH-1–CLDH-9.

Material	Weight ratio [wt%]	s_{top}	s_{side}	$rmsd_{top}$ [Å]	$rmsd_{side}$ [Å]
CLDH-1	73.29	0	4.80	0.15	0.21
CLDH-2	71.37	0	4.92	0.25	0.26
CLDH-3	69.44	0	3.23	0.35	0.75
CLDH-4	67.52	0	3.38	0.28	0.66
CLDH-5	65.60	0	2.72	0.41	0.71
CLDH-6	63.68	0	1.32	0.53	1.01
CLDH-7	61.75	0	1.04	0.36	1.24
CLDH-8	59.83	0.05	0.40	0.64	1.31
CLDH-9	57.91	0.12	0.83	1.48	1.48

© 2016 Wiley-VCH Verlag GmbH & Co. KGaA, Weinheim

S_{side}, S_{top}, and rmsd are summarized in Table 1. It is surprisingly that the value of S_{top} for CLDH-*n* (*n* = 1–6) is always zero, which indicates the highly uniform distribution of metal atoms in the LDH (001) facet during the structural evolution process at 450 °C. Additionally, the low $rmsd_{top}$ values (0.15–0.53 Å) for CLDH-*n* (*n* = 1–6) demonstrate that the metal atoms in the host layers in the LDH (001) facet do not migrate from their original position in the initial LDH model. The value of S_{side} gradually decreases from 4.80 (CLDH-1) to 2.72 (CLDH-5), which implies that the metal cations mainly aggregate in the host layer and gradually spread to the interlayer region as the dehydration reaction proceeds. This is confirmed by the modest $rmsd_{side}$ values, which increase from 0.21 (CLDH-1) to 0.71 Å (CLDH-5). However, the values of both S_{side} and $rmsd_{side}$ vary sharply when CLHD-5 is dehydrated to CLDH-6 (Table 1): the value of S_{side} suddenly falls down by more than 50%, from 2.72 to 1.32; the $rmsd_{side}$ increases by 42% from 0.71 to 1.01 Å. This suggests that the metal atoms substantially shift to the interlayer region along the *c*-axis direction perpendicular to the (001) facet, which results in the decentralization of metal atoms in the LDH (120) facet (side view). It is noteworthy that the Al atoms display much lower mobility than the Mg atoms (Figure 8D), mainly due to the stronger electrostatic attraction between Al^{3+} and O^{2-}/OH^{-}. This suggests that Al^{3+} can stabilize the layered structure; therefore, the topotactic transformation of LDH precursors with a higher Mg/Al ratio will start at low temperatures. Kanezaki's work also confirmed that the transition temperatures of LDHs with Mg/Al ratios of 3 and 4 are lower than that of Mg/Al = 2 by 20 and 40 °C, respectively.[28] Based on the S_{top}, S_{side}, $rmsd_{side}$, and $rmsd_{top}$ results, the structural evolution process during the decomposition of LDHs at 450 °C can be determined as follows: metal cations are almost fixed within the LDH (001) facet during thermal decomposition, but they prominently migrate in the direction perpendicular to the (001) facet. This can explain the template effect of LDH precursors in the preparation of highly dispersed metal nanoparticles through the topotactic transformation. In addition, the disappearance of the memory effect when CLDH-5 is dehydrated to form CLDH-6 can be attributed to the prominent migration of metal cations in the direction of the *c* axis, but not along the direction of the *a* and *b* axes; this leads to substantial damage to the layered structure.

2.5. DFT Simulation of the Structural Evolution of LDHs at 800 °C

The structure of CLDH-7 was simulated at 800 °C, and subsequently dehydrated to CLDH-8 ($H_4O_{16}Mg_8Al_4$), -9 ($H_2O_{15}Mg_8Al_4$), and -10 ($O_{14}Mg_8Al_4$). According to the low values of S_{top} and $rmsd_{top}$ for CLDH-7 and -8 (Table 1), the arrangement of metal cations in the LDH (001) facet (Figure 9A and B) mainly retains the same distribution as that in the initial LDHs. When CLDH-8 loses a water molecule, only two hydroxyl groups are removed from the system (CLDH-9; Figure 9C). According to the results,

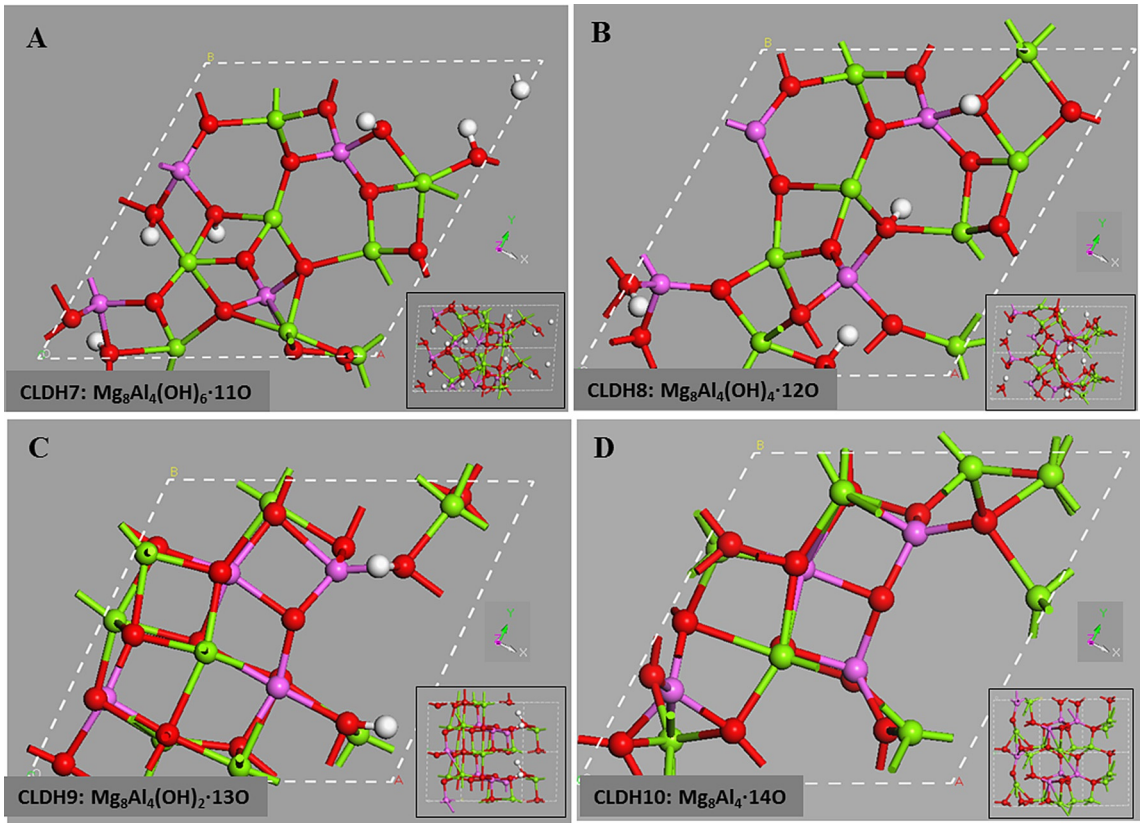

Figure 9. Snapshots of the *NVT* (800 °C) dynamic simulations of A) CLDH-7, B) CLDH-8, C) CLDH-9, and D) CLDH-10 (white, H; gray, C; red, O; green, Mg; pink, Al). The inserts show the side views of the corresponding structures.

© 2016 Wiley-VCH Verlag GmbH & Co. KGaA, Weinheim

both Mg^{2+} and Al^{3+} in CLDH-9 are six-coordinated and show a similar arrangement to that of Mg^{2+} in MgO, except for those in the vacancy. The value of S_{top} for CLDH-9 rises to 0.12, and the $rmsd_{top}$ value becomes as high as 1.48 Å, which indicates that the arrangement of metal cations is completely different from that in the initial LDHs. It is noteworthy that Al^{3+} cations in CLDH-9 are linked together by bridge oxygen atoms rather than maintain a high distribution in ideal LDHs. According to the in situ XRD data, the final product of LDHs at 800 °C is composed by amorphous MMOs. The model used in the calculation is clearly too limited to simulate this amorphous solid, but the structures of CLDH-9 and -10 still reflect some properties of the products: 1) collapse of the Mg_2Al–CO_3 LDH at 800 °C leads to many holes, as experimentally confirmed by the N_2 adsorption/desorption isotherms of the Mg_2Al and calcined LDHs (Figure S5, Supporting Information). Specifically, the MMO exhibits a larger specific surface area (125.5 m^2g^{-1}), much larger than that of pristine LDH nanoplatelets (71.8 m^2g^{-1}), which is similar to a previously reported result.[54–56] In addition, pore size analysis based on the isotherms illustrated that two samples possessed a mesopore distribution in the range of 3–10 nm. 2) The Mg^{2+} cations tend to accumulate and transform into tiny MgO crystals.

2.6. Calculated XRD pattern of the Intermediates in Comparison with the Experimental Results

To validate the simulated structures of the intermediates at different temperatures, the experimentally observed in situ XRD results are compared with the XRD patterns of the simulated structures at 230, 330, 450, and 800 °C (Figure 10). As shown in Figure 10 A, the calculated XRD pattern of $Mg_8Al_4(OH)_{24}{\cdot}2CO_3$ nicely reproduces the experimental results, and displays a clear peak at $2q = 13.2°$ ($d = 6.70$ Å). This indicates that most of the crystalline water in the LDH sample has been removed at around 230 °C and the layered host–guest structure is well preserved. At 330 °C, the in situ XRD pattern of the calcined sample shows a wide peak at $2q = 22.0°$, and the calculated data also has a clear peak at about 21.0° with a narrow peak width (Figure 10 B). This implies that the simulated result can essentially reflect the structure of the calcined LDH sample at this temperature. The structure of $Mg_8Al_4(OH)_{20}{\cdot}4O$ obtained by MD simulation is an ideal model with a regular crystal lattice, but, during the practical calcination of the LDH sample, the decomposition of Mono-LDH is substantially affected by defects (especially the edges of the sheets), and thus, proceeds irregularly; therefore, the interlayer distance varies over a wide range. This leads to much wider XRD peaks in the experimental curve than those in the calculated one (Figure 10 B). As shown in Figure 10 C, the simulated XRD patterns of CLDH-5 and -6 at 450 °C are very complicated, and a number of peaks appear in the range of 17–70°. This is because the layered

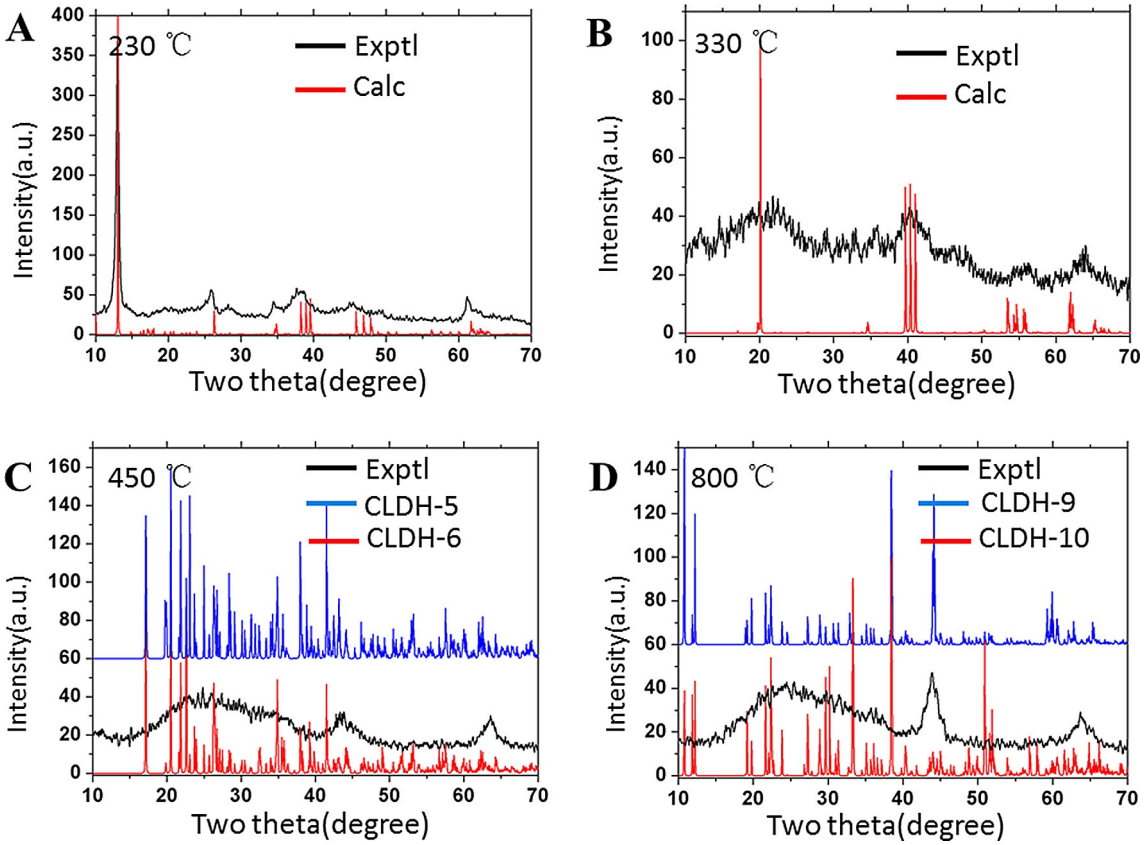

Figure 10. Calculated XRD patterns of the simulated intermediates and corresponding experimental results at A) 230, B) 330, C) 450, and D) 800 °C.

© 2016 Wiley-VCH Verlag GmbH & Co. KGaA, Weinheim

structures of the simulated models are largely destroyed and the structures become inhomogeneous. The experimentally observed in situ XRD pattern displays a wide peak from 15 to 38° with the maximum located at 25°. In the same range, the simulated XRD patterns of CLDH-5 and -6 show the highest intensity at around 23°, which is consistent with the experimental data. Additionally, the experimental XRD curve displays a clear peak at 44° ($d=2.06$ Å), which is attributed to the MgO phase, in accordance with previous reports.[28] The XRD pattern of CLDH-5 shows a high-intensity peak at 42.5° ($d=2.12$ Å), which is mainly caused by the migration of the metal cations. This may lead to the final formation of the MgO phase in the decomposition of the LDH sample. In terms of the XRD results, the simulated structures (CLDH-5 and -6) can essentially reproduce the experimentally calcined product; this supports the dependability of the calculated results. At 800 °C, the experimental XRD result shows a similar pattern to that at 450 °C, but with a higher peak at 44°, which suggests the further formation of the MgO phase. The simulated XRD pattern of CLDH-10 is significantly different from that of the experimental results; however, the simulated XRD results of LDH-9 are more consistent with the observed pattern, except that the calculated XRD pattern of CLDH-9 also displays a high peak at 38°. This peak is mainly contributed to by the elongation of the Mg–O bonds in the simulated model. Considering that the metal cations in CLDH-9 have a similar arrangement of Mg^{2+} in MgO, the in situ XRD results suggest that the structure of CLDH-9 is more reliable than that of CLDH-10 because the present models are still too limited to simulate the structural evolution process at high temperature.

3. Conclusions

DFT calculations and experimental studies were performed to investigate the thermal decomposition mechanism of MgAl LDHs. TG-DTA results for carbonate-intercalated MgAl LDHs indicated that the crystal displayed three apparent endothermic peaks at 230, 330, and 450 °C. The MD simulation results showed that LDH decomposed into CO_2 and water through a monodentate configuration at 330 °C, but nicely preserved its layered structure. At 450 °C, the dehydration process of the LDHs was calculated by MD simulations and the resulting structures showed that the metal cations were fixed in their original position within the LDH(001) facet during the topotactic structural evolution process, but migrated substantially along the *c*-axis direction. In addition, this migration finally led to the disappearance of the memory effect and damage to the layered structure. Simulation results at 800 °C indicated that the collapsed layered structure led to many holes and the distribution of metal cations was completely different from that in LDHs. Finally, the simulated structures were validated by the experimentally observed in situ XRD data. This work provided a fundamental insight into topotactic transformation in the thermal decomposition process of MgAl LDHs; this is helpful for the exploration and fabrication of supported metal catalysts and related functional materials.

Finally, it is noteworthy that the thermal decomposition of LDHs was strongly affected by the interlamellar anions and the metal composition of the layers. The difference mainly lay in the decomposition temperature of different stages and structures of the calcined products.[32,51,65–67] In subsequent work, we will carry out a topotactic transformation study on transition-metal-containing LDHs and expect to obtain some more useful results to extend the applicability of this process for the preparation of nanocatalysts in the future.

Experimental Section

Materials

Analytical grade chemicals, including ethanol, $Mg(NO_3)_2{\cdot}6H_2O$, $Al(NO_3)_3{\cdot}9H_2O$, and urea were used without further purification. Deionized water was used in all experimental processes.

Preparation of LDH

LDH platelets were prepared by the previously reported coprecipitation method through urea hydrolysis with hydrothermal treatment.[36] Typically, 0.005 M $Al(NO_3)_3{\cdot}9H_2O$, 0.01 M $Mg(NO_3)_2{\cdot}6H_2O$, and 0.05 M $CO(NH_2)_2$ were dissolved in deionized water (150 mL) and transferred into a Teflon-lined stainless-steel autoclave. Subsequently, the autoclave was sealed and hydrothermally treated at 110 °C for 24 h. The resulting LDH powder was obtained by centrifugation and washed with water and ethanol several times, then dried at 60 °C for 12 h. This method has been widely employed for preparing LDH samples ($Mg_8Al_4(OH)_{24}{\cdot}2CO_3{\cdot}6H_2O$) with high purity and crystallinity.[57,58]

Calcination of LDH to MMO

The obtained LDH sample was calcined in air in the range of 100–800 °C for 3 h at a heating rate of 2 °C min^{-1}. After calcination in the temperature range of 500–800 °C, LDH was transformed into MMOs with a porous structure.

Sample Characterization

XRD patterns were recorded by using a Rigaku XRD-6000 diffractometer with Cu Ka radiation ($l=0.1542$ nm) at 40 kV and 30 mA. TG-DTA curves were obtained on a Beifen PCT-IA instrument in the temperature range of 30–800 °C. The morphology was investigated by using a scanning electron microscope (Zeiss SUPRA 55), with an accelerating voltage of 20 kV, and an FEI Cs-corrected Titan 80–300 high-resolution transmission electron microscope operated at 300 kV. The specific surface area was determined based on the BET method by using a Quantachrome Autosorb-IC-VP analyzer.

Computational Models

The model of Mg_2Al–CO_3 LDH was established in accordance with the reported crystal data.[59] The supercell model was $2\sqrt{3}\times2\sqrt{3}\times1$ in the *a*, *b*, and *c* directions, respectively, containing $8Mg^{2+}$, $4Al^{3+}$, and $24OH^-$ groups in each octahedral layer and $2CO_3^{2-}$ and $6H_2O$ in the interlayer region ($Mg_8Al_4(OH)_{24}{\cdot}2CO_3{\cdot}6H_2O$; Figure 11). The initial lattice parameters were $a=b=10.53$ Å, $c=7.49$ Å (experimental values). One of the most important theoretical focuses in the present study was on the migration and distribution of

© 2016 Wiley-VCH Verlag GmbH & Co. KGaA, Weinheim

metal cations in the structural evolution process of the LDH; therefore, the Mg/Al ratio was selected to be two; this is the most commonly used LDH and the most economical model containing enough Mg and Al atoms (at least 2 Al atoms in each layer) to study the migration mechanism.

Computational Methods

DFT calculations were performed by using the Vienna ab initio simulation package (VASP).[60,61] The gradient-corrected exchange/correlation functional of Perdew and Wang was employed, and a plane-wave basis with a 400 eV kinetic-energy cutoff was adopted to describe electronic states by using the projector augmented wave (PAW) basis set.[57] The self-consistent field (SCF) converged criterion was within 1.0×10^{-5} eV and the convergence criterion of the structure optimization was 1.0×10^{-5} eV. Brillouin zone sampling was performed by using a $1\times1\times1$ *k*-point mesh in the structural simulations. The pressure was set to be 0.1 MPa, and the *k*-point sample of $4\times4\times4$ was employed during the vibration calculation. To dynamically study the structural evolution of LDH decomposition, DFT-based MD calculations were performed in the canonical ensemble (*NVT*) by using the Nosé algorithm, which has been widely used in MD simulations of solid materials.[37,62–64] The time step was 1 fs with total simulation times of up to 30 ps, which was long enough to perform the DFT-based MD simulation.[17]

Acknowledgements

This work was supported by the 973 Program (grant no.: 2014CB932101), the National Natural Science Foundation of China (NSFC), the Fundamental Research Funds for the Central Universities (YS 1406), and the Specialized Research Fund for the Doctoral Program of Higher Education (20130010110013). M.W. particularly appreciates financial aid from the China National Funds for Distinguished Young Scientists of the NSFC. We acknowledge the National Supercomputing Center in Shenzhen and the "Chemical Grid Project" of Beijing University of Chemical Technology for providing the computational resources.

Keywords: aluminum · density functional calculations · layered double hydroxides · magnesium · structure elucidation

[1] X. Duan, D. G. Evans, *Layered Double Hydroxides: Structure and Bonding*, Springer, Berlin, **2006**.
[2] G. R. Williams, D. O'Hare, *J. Mater. Chem.* **2006**, *16*, 3065 – 3074.
[3] L. Mohapatra, K. M. Parida, *Phys. Chem. Chem. Phys.* **2014**, *16*, 16985 –